Characterization of an HMG-CoA Reductase from *Listeria monocytogenes* That Exhibits Dual Coenzyme Specificity

Amy E. Theivagt,[‡] Elise N. Amanti,[‡] Nicola J. Beresford,[§] Lydia Tabernero,[§] and Jon A. Friesen*[,‡]

Department of Chemistry, Illinois State University, Normal, Illinois 61790, and School of Biological Sciences, University of Manchester, Manchester M13 9PT, United Kingdom

Received July 19, 2006; Revised Manuscript Received September 27, 2006

ABSTRACT: HMG-CoA reductase (HMGR) is an enzyme critical for cellular cholesterol synthesis in mammals and isoprenoid synthesis in certain eubacteria, catalyzing the NAD(P)H-dependent reduction of HMG-CoA to mevalonate. We have isolated the gene encoding HMG-CoA reductase from *Listeria monocytogenes* and expressed the recombinant 6×-His-tagged form in *Escherichia coli*. Using NAD(P)(H), the enzyme catalyzes HMG-CoA reduction approximately 200-fold more efficiently than mevalonate oxidation in vitro. The purified enzyme exhibits dual coenzyme specificity, utilizing both NAD(H) and NADP(H) in catalysis; however, catalytic efficiency using NADP(H) is approximately 200 times greater than when using NAD(H). The statins mevinolin and mevastatin are weak inhibitors of *L. monocytogenes* HMG-CoA reductase, requiring micromolar concentrations for inhibition. Three-dimensional modeling reveals that the overall structure of *L. monocytogenes* HMG-CoA reductase is likely similar to the known structure of the class II enzyme from *Pseudomonas mevalonii*. It appears that the enzyme has catalytic amino acids in analogous positions that likely play similar roles and also has a flap domain that brings a catalytic histidine into the active site. However, in *L. monocytogenes* HMG-CoA reductase histidine 143 and methionine 186 are present in the putative NAD(P)(H)-selective site, possibly interacting with the 2′ phosphate of NADP(H) or 2′ hydroxyl of NAD(H) and providing the active site architecture necessary for dual coenzyme specificity.

Isopentenyl pyrophosphate (IPP), the product of the mevalonate pathway (Figure 1), is central to the biosynthesis of countless isoprenoids by eukarya, archaea, and certain eubacteria including rubber, carotenoids, dolichols, polyisoprenoids of cell walls, cholesterol and other sterols. The enzyme 3-hydroxy-3-methylglutaryl coenzyme A reductase (HMG-CoA reductase, HMGR, EC 1.1.1.34) catalyzes the four-electron reduction of HMG-CoA to mevalonate, a reaction central to IPP synthesis. HMGR in mammals serves as the rate-limiting enzyme of cholesterol biosynthesis and is the target of anticholesterolemic agents such as statin drugs. HMGRs are divided into two classes based on primary structure, sequence alignments, and sensitivity to statins (*1*). Class I enzymes include eukaryotes and most archaea and are inhibited by statin drugs in the nanomolar concentration range. Class I forms of HMGR that have been characterized include human (*2*), Syrian hamster (*3*), the yeast *Saccharomyces cerevisiae* (*4*), the halophile *Haloferax volcanii* (*5*), and the thermophile *Sulfolobus solfataricus* (*6*). Class II forms of HMG-CoA reductase are much less sensitive to statins, requiring micromolar concentrations for inhibition, and are utilized by prokaryotes and certain archaea (*7*). Characterized class II HMGRs include those from *Pseudomonas mevalonii* (*8*), *Streptomyces sp* (*9*), *Staphylococcus aureus* (*10*), and *Archeoglobus fulgidus* (*11*). *Pseudomonas mevalonii*, a soil bacterium, utilizes HMG-CoA reductase in a biodegradative role, allowing for the use of mevalonate as a carbon source during growth (*12*). Accordingly, HMG-CoA lyase, an enzyme that catalyzes the degradation of mevalonate, is found in an operon along with HMG-CoA reductase in *P. mevalonii*. The structure of *P. mevalonii* HMGR has been solved and serves as a model structure for class II forms of the enzyme (*13*, *14*). Other prokaryotes, however, appear to utilize HMG-CoA reductase biosynthetically for the eventual synthesis of monoterpenes, carotenoids, quinones, and membrane components. For recent reviews on HMG-CoA reductase, refer to refs *7*, *15*, and *16*.

The mevalonate pathway is not the only known route for the synthesis of IPP; the methylerythritol 4-phosphate (MEP) pathway, also known as the 1-deoxy-D-xylulose 5-phosphate (DXP or DOXP) pathway or the Rohmer pathway, has been elucidated (*17*). The pathway is initiated by the condensation of glyceraldehyde 3-phosphate and pyruvate. Non-photosynthetic eukaryotes and archaea appear to use only the mevalonate pathway for IPP synthesis. With the exception of the unicellular green algae, which use the DOXP pathway exclusively, plants and algae operate the mevalonate pathway in the cytoplasm and the DOXP pathway in the chloroplast. Eubacteria, depending on the species, appear to utilize either pathway or, in some cases, both pathways. For recent reviews on IPP biosynthesis, including genomic analysis of pathway enzymes, refer to refs *18* and *19*.

Listeria monocytogenes, a gram positive rod-shaped bacterium, is an opportunistic pathogen known to cause the

* Corresponding author. Telephone: (309) 438-7850. Fax: (309) 438-5538. E-mail: jfriese@ilstu.edu.

[‡] Illinois State University.

[§] University of Manchester.

10.1021/bi0614636 CCC: $33.50
Published on Web 11/09/2006

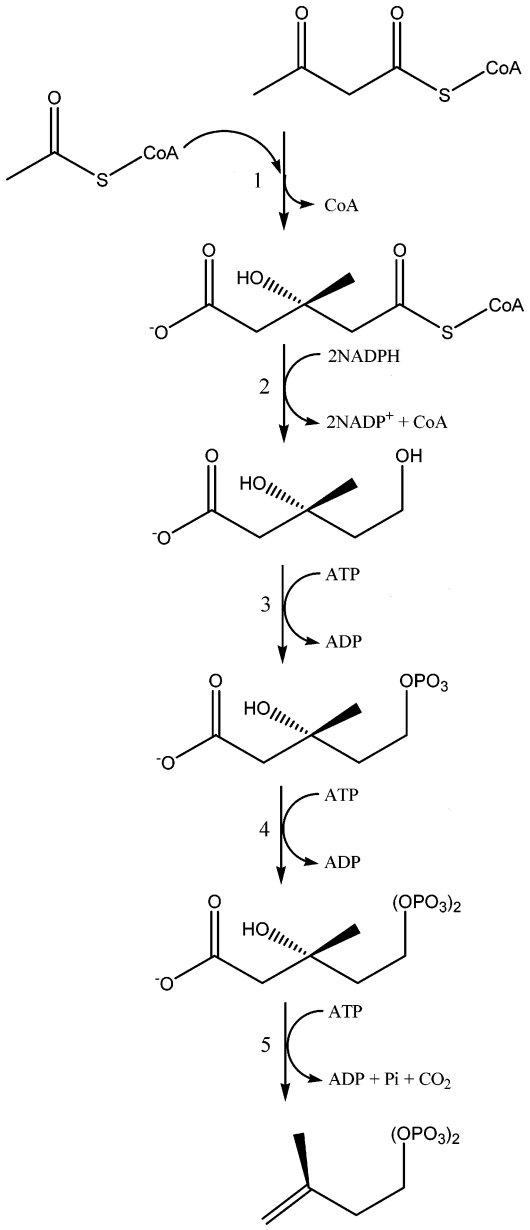

FIGURE 1: The mevalonate pathway. Synthesis of isopentenyl pyrophosphate (IPP) is achieved via the sequential action of five enzymes: (1) HMG-CoA synthase, which condenses acetoacetyl-CoA and acetyl-CoA to form HMG-CoA, (2) HMG-CoA reductase, which reduces HMG-CoA to mevalonate, (3) mevalonate kinase, which phosphorylates mevalonate, (4) phosphomevalonate kinase, which catalyzes a second phosphorylation, and (5) mevalonate pyrophosphate decarboxylase, which produces isopentenyl pyrophosphate. The figure was constructed using ChemDraw 7.0.

disease listeriosis, potentially fatal in humans, especially in the case of immunocompromised individuals, infants, or pregnant women. This food-borne pathogen is potentially dangerous for humans since it is able to survive in relatively high temperatures and high salt concentrations as well as tolerate high bile acid concentrations (*20*). The organism initially infects the intestines, causing gastroenteritis, and can eventually cause septicemia or make its way to the placenta and/or central nervous system, with the potential to result in meningitis and encephalitis. The recent sequencing of the *Listeria monocytogenes* genome (*21*) will likely facilitate characterization of enzymes and metabolic pathways to serve as targets against Listeria and increase the safety of the food supply. Class II HMG-CoA reductases of pathogenic bacteria may hold promise as a target for antibiotic compounds due to the structural and catalytic differences when compared to class I enzymes of eukaryotes. Differences in structure, regulation, and sensitivity to statins between the two classes may allow for designing antibiotics that target only a class II enzyme (*22*).

We describe in this report the characterization of HMGR from *Listeria monocytogenes*. The gene encoding the enzyme has been amplified from genomic DNA and expressed in *Escherichia coli* as a 6×-His-tagged form, producing milligram quantities of purified recombinant enzyme. Kinetic characterization has been conducted and HMGR is shown to utilize both NAD(H) and NADP(H) for catalysis. *L. monocytogenes* HMGR appears to be a class II HMGR based on sensitivity to statins, primary structure, and three-dimensional (3D) structural modeling.

EXPERIMENTAL PROCEDURES

Polymerase Chain Reaction. A culture of *Listeria monocytogenes* EGD-e (a gift from Dr. Brian Wilkinson, Department of Biological Sciences, Illinois State University) was used to prepare genomic DNA using a Promega Wizard Genomic DNA Extraction kit. Oligonucleotides were designed that would amplify the full-length gene encoding *L. monocytogenes* HMG-CoA reductase with a BamHI site (underlined) at the 5′ end (5′-ACCATGGATCCCCACGTGAATGCTTTTGATAAATTTTATAAAAAAACAG-3′) and a NotI site (underlined) at the 3′ end (5′-GCGATTACGCGGCCGCGTCGACTTATTTTTCGCTGCGCAATTTCGCG-3′). PCR was conducted using the following concentrations of reagents: 1 μM each oligonucleotide, 0.25 mM each dNTP, 1 ng of genomic DNA, 1 unit *Pfx* DNA polymerase (Invitrogen), and between 1 and 8 mM $MgSO_4$. Thermocycle parameters were as follows: 94 °C 15 s, 52 °C 15 s, and 68 °C 1 min for 30 cycles. The approximately 1.28 kbp PCR product was cloned into pET45b (Novagen), using the BamHI and NotI restriction sites of the multiple cloning site, producing the recombinant plasmid denoted pET45b-LmHMGR. Cloning into pET45b appends a nucleotide sequence to the gene encoding an additional 24 amino acids (MAHHHHHHVGTGSNDDDDKSPDPH) at the amino terminus that includes a 6×-His-tag. The DNA sequence of the *L. monocytogenes* HMGR gene was determined using automated DNA sequencing with fluorescent ddNTP dye terminators.

Expression of L. monocytogenes HMG-CoA Reductase. Competent BL21(DE3)RIL *E. coli* (Novagen) were transformed with pET45b-LmHMGR and grown on LB agar plates containing 100 μg/mL ampicillin and 34 μg/mL chloramphenicol. Colonies were selected and placed into 5 mL of LB media containing antibiotics. Following growth at 37 °C for 16 h while shaking at 250 rpm, cultures were transferred to one liter of LB containing antibiotics and growth was continued at 37 °C, 250 rpm until the optical density at 600 nm reached a value of approximately 0.8. Isopropylthiogalactopyranoside (IPTG) was added to a concentration of 1 mM and cultures were incubated an additional 3 h at 37 °C, 250 rpm. Cells were harvested by centrifugation at 5000*g* for 5 min, resuspended in 20 mL of buffer A (20 mM Tris-Cl, pH 7.5, 100 mM NaCl), and lysed

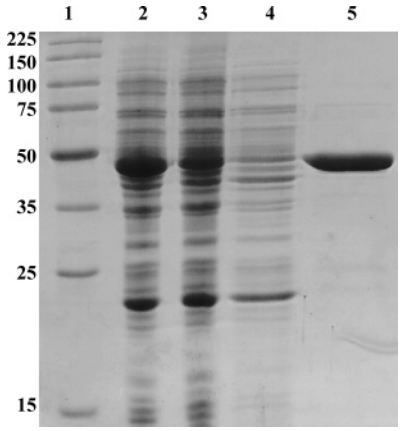

FIGURE 2: Purification of 6×-His-tagged *L. monocytogenes* HMG-CoA reductase. Lane 1: Molecular weight standards (kDa). Lane 2: cell lysate. Lane 3: 100000*g* cell supernatant. Lane 4: buffer A column wash. Lane 5: 150 mM imidazole in buffer A elution.

using a French Press at 20 000 psi. The cell lysate was centrifuged at 100000*g* for 30 min, and the supernatant fraction was utilized for protein purification.

Purification of L. monocytogenes HMG-CoA Reductase. Purification of 6×-His-tagged *L. monocytogenes* HMGR was accomplished using affinity chromatography on TALON Co^{2+} metal affinity resin (Clontech). The 100000*g* cell supernatant fraction was loaded onto a 1.5 × 1.5 cm Co^{2+} metal affinity column equilibrated with buffer A. The column was washed with 10 column volumes of buffer A followed by 10 column volumes of buffer A containing 10 mM imidazole. The enzyme was eluted from the column in 1 mL fractions with 10 mL buffer A containing 150 mM imidazole. Protein was determined by the method of Bradford (*23*) using bovine serum albumin as standard and a Protein Assay kit from Bio-Rad. Purification consistently resulted in greater than 20 mg of pure protein per liter of bacterial culture. The 6×-His-tagged enzyme was electrophoretically pure and migrated as a single band of approximately 48 kDa on SDS−PAGE (Figure 2). The calculated molecular mass of the 6×-His-tagged form of the enzyme is 48.3 kDa. Upon purification the enzyme exhibited a specific activity between 15 and 20 μmol of NADPH oxidized min^{-1} (mg of enzyme)$^{-1}$.

Enzyme Assays. L. monocytogenes HMG-CoA reductase was assayed essentially as described previously (*16*). For mevalonate oxidation, a standard reaction mixture contained 8 mM Tris-Cl, 8 mM KCl, 4 mM $NADP^+$, 6 mM mevalonate, 2 mM CoA, and enzyme in a final volume of 150 μL at pH 8.5. For HMG-CoA reduction, a standard reaction mixture contained 8 mM Tris-Cl, 8 mM KCl, 0.13 mM NAD(P)H, 0.17 mM HMG-CoA, and enzyme in a final volume of 150 μL at pH 7.0. Reactions were at 37 °C for 30 s in an HP8453a spectrophotometer with a temperature-controlled cuvette holder.

Kinetic Analysis. The kinetic parameters V_{max} and K_m with respect to substrates were determined using primary plots of initial velocity (v_o) versus substrate concentration [S]. Data were analyzed by nonlinear regression using SigmaPlot (Systat Software, Inc.). Initial velocity versus [S] data were fit to the Hill equation, $v_o = (V_{max}[S]^b)/(K'^{,b} + [S]^b)$, where v_o is the initial velocity, K' is the concentration of substrate eliciting half-maximal velocity, and b is the Hill coefficient (*24*). For inhibition studies, *L. monocytogenes* HMGR was assayed in the presence of mevinolin or mevastatin (compactin) at the indicated concentrations, up to 0.25 mM, and initial velocity data were plotted versus inhibitor concentration. The lactone form of each statin was dissolved in DMSO, and the acid forms were produced by placing the compounds in 250 mM NaOH for 1 h at 37 °C (*25*).

Dynamic Light Scattering. Multi-angle laser light scattering (MALLS) was performed on a Wyatt EOS laser photometer with a 688 nm laser and Wyatt Optilab refractometer. This was coupled to a Dionex Bio LC HPLC. The recombinant Listeria HMGR sample at 0.2 mg/mL was passed through a Superdex 200 (Amersham) 24/30 gel filtration column at 0.5 mL/min in 10 mM Tris, 100 mM NaCl, pH 7.5.

Modeling of the Three-Dimensional Structure of L. monocytogenes HMG-CoA Reductase. A homology model of *L. monocytogenes* HMGR was built with SegMod (*26*) using an amino acid sequence alignment and the ternary complex structure of *P. mevalonii* HMGR (*14*). A dimer of *L. monocytogenes* HMGR was built that contained two flap domains followed by conjugate gradient minimization of the final dimeric structure using CNS (*27*) to remove unfavorable contacts and electrostatic repulsions. Docking of the substrate HMG-CoA and cofactor NAD^+ in the putative active site was performed using the coordinates from the *P. mevalonii* HMGR ternary complex and further refined with CNS, using polar hydrogens built on the protein and substrate molecules.

RESULTS AND DISCUSSION

The L. monocytogenes HMGR Gene Encodes a 426 Amino Acid Polypeptide. The gene encoding HMGR in *L. monocytogenes* is found at location 851225−852505 of the 2.94 Mbp *L. monocytogenes* genome (GeneID: 985372). PCR amplification utilizing a *L. monocytogenes* genomic DNA preparation as template resulted in a 1.3 kb pair double-stranded DNA product, the approximate size predicted for the full-length gene encoding HMG-CoA reductase. Upon ligation of the DNA fragment into pET45b, the amplified DNA was sequenced and found to contain a 1281 nucleotide base pair open reading frame encoding HMGR that matched the genome sequence for *L. monocytogenes* strain EGD except for a thymine at position 114 that was reported as a guanine in the database sequence (accession NC_003210). However, each of the resulting codons (GCT and GCG) coded for alanine. Therefore, the encoded amino acid sequence translated from the gene sequence agrees with the database sequence.

The *L. monocytogenes* HMG-CoA redutase gene encodes a 426 amino acid polypeptide with a calculated molecular mass of 45 854 Da (protein id NP_464352, hypothetical protein lmo0825). Amino acids previously shown to be critical for catalysis in other forms of HMGR appear to be conserved in *L. monocytogenes* HMG-CoA reductase, including Glu80, Lys264, Asp280, and His378, which correspond to Glu83 (*28*), Lys267 (*29*), Asp283, and His381 (*30*) of *Pseudomonas mevalonii* HMGR. The conservation of catalytic amino acids suggests that *L. monocytogenes* HMGR possesses a catalytic mechanism similar to other HMGRs. Predictably, sequence alignment also suggests that *L. monocytogenes* HMGR does not possess a phosphorylat-

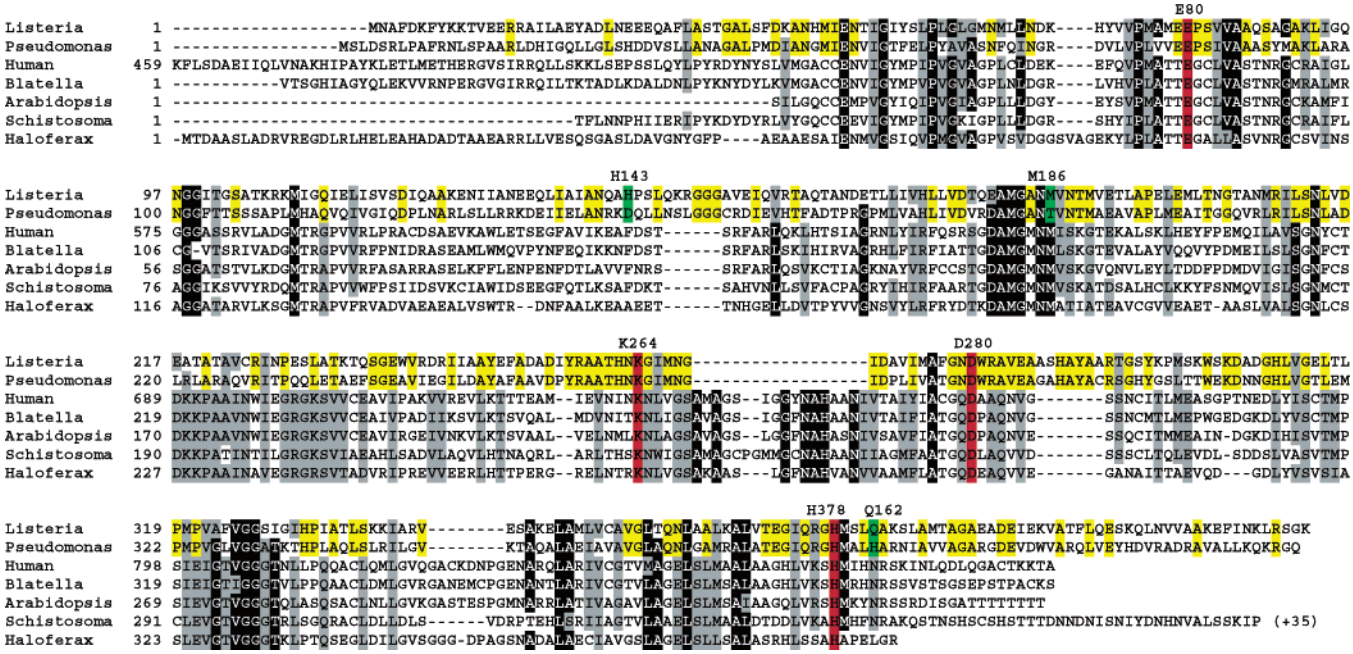

FIGURE 3: Comparison of the amino acid sequence of *L. monocytogenes* HMGR to other HMG-CoA reductases. Boxed in black are amino acids identical in at least five of the seven HMGRs. Boxed in gray are amino acids similar in at least five of the seven HMGRs. Boxed in yellow are amino acids conserved between *L. monocytogenes* HMGR and *Pseudomonas mevalonii* HMGR, the two class II HMGRs in the alignment. Noted in red are putative active site amino acids Glu80, Lys264, Asp280, and His378 of *L. monocytogenes* HMGR, shown previously to be critical for catalysis by other HMGRs. Highlighted in green are His143 and Met186, amino acids in the NAD(P)(H)-selective site in the 3D structural model. Other HMG-CoA reductase sequences are *Pseudomonas mevalonii* HMGR (accession AAA25837), human HMGR (accession NP_000850), *Blatella germanica* (cockroach) HMGR (accession CAA49628), *Arabidopsis thaliana* HMGR (accession NP_177775), *Schistosoma mansoni* HMGR (accession AAA29896), and *Haloferax volcanii* HMGR (accession AAA73174).

able serine (Ser 871 of hamster HMGR) that mediates reversible regulation of mammalian HMGRs (*31*).

Listeria monocytogenes Contains a Class II HMG-CoA Reductase. Inspection of multiple sequence alignments and inhibitor studies permitted Bochar et al. (*1*) to identify two classes of HMGR. Sequence conservation within each class is significantly higher than between classes. The enzymes of class I include all eukaryotic HMGRs and several archaeal enzymes, while the class II enzymes are eubacterial or archaeal. An alignment comparing the *L. monocytogenes* HMGR amino acid sequence to other HMG-CoA reductases is shown in Figure 3. Upon alignment with class II HMGRs, the amino acid sequence of *L. monocytogenes* HMGR is 44% identical to *P. mevalonii* HMGR, 42% identical to *Staphylococcus aureus* HMGR, and 45% identical to *Archaeoglobus fulgidus* HMGR. When compared to class I HMGRs, *L. monocytogenes* HMGR is 15% identical to the catalytic domains of human, *Arabidopsis thaliana*, and *Haloferax volcanii* HMGRs and 18% identical to the catalytic domains of *Saccharomyces cerevisiae* and *Sulfolobus solfataricus* HMGRs. Sequence alignment, therefore, suggests *L. monocytogenes* possesses a Class II HMGR, an observation that would later be confirmed by biochemical analysis.

L. monocytogenes HMG-CoA Reductase Exhibits Dual Coenzyme Specificity. Enzyme assays were conducted to determine the ability of *L. monocytogenes* HMG-CoA reductase to catalyze each of the following four reactions: HMG-CoA reduction using NADPH, HMG-CoA reduction using NADH, mevalonate oxidation using $NADP^+$, and mevalonate oxidation using NAD^+. Initial assays revealed that *L. monocytogenes* HMGR readily catalyzed HMG-CoA reduction at a pH optimum of 7.0 (data not shown) with either NADPH or NADH, although it was evident that the rate of reaction was significantly greater using NADPH. Steady-state kinetic characterization revealed the V_{max} to be 18.2 μmol of NADPH oxidized min^{-1} (mg enzyme)$^{-1}$ or 0.78 μmol of NADH oxidized min^{-1} (mg enzyme)$^{-1}$. The K' value for HMG-CoA was 19.8 μM (using NADPH) and 13.4 μM (using NADH), with Hill constants of 2.20 and 1.82, respectively. The K' value for NADPH was 12.9 μM with a Hill coefficient of 2.21, and the K' value for NADH was 150 μM with a Hill coefficient of 0.97 (Table 1). The Hill coefficient values greater than 1.0 indicate cooperativity toward HMG-CoA and NADPH but not NADH.

The rate of catalysis for mevalonate oxidation was significantly less than HMG-CoA reduction using either $NADP^+$ or NAD^+ in the presence of CoA. The optimal pH for mevalonate oxidation was approximately 8.5 (data not shown). Kinetic analysis revealed the V_{max} to be 2.97 μmol of $NADP^+$ reduced min^{-1} (mg of enzyme)$^{-1}$ or 0.99 μmol of NAD^+ reduced min^{-1} (mg of enzyme)$^{-1}$. The K' value for $NADP^+$ was 445 μM and for NAD^+ was 25 000 μM. The K' value for mevalonate was 427 μM, while the K' value for CoA was 145 μM using $NADP^+$ as oxidant (Table 1). K' values were not determined for mevalonate and CoA in the presence of NAD^+ since the high K' value for NAD^+ prevented conducting the assay at saturating NAD^+ concentrations. Fitting the data to the Hill equation indicated little to no cooperativity toward substrates, with Hill coefficients between 1.05 and 1.25.

Comparison of Kinetic Properties of L. monocytogenes HMG-CoA Reductase to Other HMG-CoA Reductases. Significant similarities as well as differences are apparent upon comparison of *L. monocytogenes* HMGR to other previously characterized HMGRs (Table 1). The V_{max} for HMG-CoA reduction of 18.2 eu/mg is similar to the class II

Table 1: Kinetic Parameters of *Listeria monocytogenes* HMG-CoA Reductase and Comparison to Representative Class I and Class II HMG-CoA Reductases[a]

	Listeria monocytogenes[b]	*Staphylococcus aureus*	*Pseudomonas mevalonii*	*Haloferax volcanii*	Syrian hamster
V_{max} (NADPH) HMG-CoA reduction	18.2 ± 0.5	21		34	64
V_{max} (NADH) HMG-CoA reduction	0.78 ± 0.15	0.9	66		
V_{max} ($NADP^+$) mevalonate oxidation	2.97 ± 0.23	3			0.6
V_{max} (NAD^+) mevalonate oxidation	0.99 ± 0.34	0.12	42		
K_m NADPH	12.9 ± 0.9	70		66	80
K_m NADH	150 ± 11	100	80		
K_m $NADP^+$	445 ± 89	580			510
K_m NAD^+	25000 ± 2180		300		
K_m HMG-CoA	19.8 ± 1.2	40	20	60	20
K_m mevalonate	427 ± 92	670	260		20
K_m coenzyme A	145 ± 19	390	60		10
ref	this study	10	16	5	16

[a] *Listeria monocytogenes* HMG-CoA reductase data were obtained and analyzed as described in Experimental Procedures and are the average of triplicate determinations. Data for other HMGRs were derived from the indicated literature reference. V_{max} is in units of eu/mg, where one enzyme unit (eu) is the nanomoles of NADH oxidized or NAD^+ reduced per minute. K_m is in units of μM. [b] For *Listeria monocytogenes* HMG-CoA reductase the K_m value is a K' value due to observed cooperativity with respect to substrates.

HMGR from *Staphylococcus aureus* (21 eu/mg) and class I HMGRs from Syrian hamster (64 eu/mg) and *Haloferax volcanii* (34 eu/mg). However, for mevalonate oxidation the V_{max} of 0.99 eu/mg is much less than the V_{max} of 42 eu/mg exhibited by *P. mevalonii* HMGR. The K' value for HMG-CoA of 19.8 μM is within 3-fold when compared to the HMG-CoA K_m values for class I and class II HMGRs. The mevalonate and CoA K' values are similar to the K_m values of other class II HMGRs but about an order of magnitude higher than HMGR from Syrian hamster.

Variation in nicotinamide coenzyme usage has been seen among the forms of HMGR characterized. The prototypical class I HMGR from Syrian hamster utilizes NADP(H), while the model enzyme for class II HMGRs from *P. mevalonii* utilizes NAD(H) as it fulfills its biodegradative role in the bacterium. *P. mevalonii* HMGR has a marked preference for NAD(H), catalyzing NAD^+-dependent mevalonate oxidation 10^6-fold more efficiently than $NADP^+$-dependent oxidation, as judged by the ratio of k_{cat}/K_m using NAD^+ to k_{cat}/K_m using $NADP^+$ (*32*).

Recently, however, forms of HMGR have been characterized that exhibit dual coenzyme specificity, from the eubacteria *Staphylococcus aureus* (*10*) and the archaebacterium *Archaeoglobus fulgidus* (*11*), which can utilize either NADP(H) or NAD(H) for catalysis. *L. monocytogenes* HMGR is very similar to *S. aureus* with respect to almost all kinetic parameters, each preferentially catalyzing NADPH-dependent HMG-CoA reduction. For both *L. monocytogenes* and *S. aureus* HMGR, the V_{max} value for HMG-CoA reduction is 23 times greater using NADPH than NADH. The main difference is the lower K_m value for NADPH exhibited by *L. monocytogenes* HMGR, making the K_m NADH/K_m NADPH ratio equal to 12, whereas *S. aureus* HMGR has almost equal K_m values for NADH and NADPH with a K_m NADH/K_m NADPH ratio of 1.4 (Table 1).

Although *L. monocytogenes* HMGR and *A. fulgidus* HMGR each are able to utilize both NAD(H) and NADP(H), their preferences are opposite of one another. *A. fulgidus* HMGR has also been extensively characterized allowing for a more detailed comparison of kinetic parameters (Table 2). *L. monocytogenes* HMGR preferentially uses $NADP^+$ for mevalonate oxidation with a k_{cat} $NADP^+/k_{cat}$ NAD^+ ratio of 3 and prefers NADPH for HMG-CoA reduction with a k_{cat} NADPH/k_{cat} NADH ratio of 23. *A. fulgidus* HMGR, however, has a 20-fold greater k_{cat} using NAD^+ and a 2-fold greater k_{cat} using NADH. Whereas *A. fulgidus* HMGR has about 3-fold higher K_m values for $NADP^+$ and NADPH than for NAD^+ and NADH, *L. monocytogenes* HMGR exhibits 56- and 12-fold higher K' values for NAD^+ and NADH than for $NADP^+$ and NADPH. Analyzing k_{cat}/K_m values illustrates that *L. monocytogenes* HMGR is approximately 200 times

Table 2: Catalytic Comparison of *Listeria monocytogenes* HMG-CoA Reductase to *Archaeoglobus fulgidus* and *Pseudomonas mevalonii* HMG-CoA Reductase

	L. monocytogenes	*A. fulgidus* (*11*)	*P. mevalonii* (*32*)
k_{cat} $NADP^+$	3.69	0.25	0.012
k_{cat} NAD^+	1.23	5.0	27
k_{cat} NADPH	22.6	1.0	
k_{cat} NADH	0.97	2.0	
K_m $NADP^+$	0.445	1.7	52
K_m NAD^+	25.0	0.50	0.21
K_m NADPH	0.0129	0.50	
K_m NADH	0.150	0.16	
k_{cat}/K_m $NADP^+$	8.29	0.147	0.00023
k_{cat}/K_m NAD^+	0.0492	10.0	129
k_{cat}/K_m NADPH	1752	2.0	
k_{cat}/K_m NADH	6.47	12.5	
k_{cat} $NADP^+/k_{cat}$ NAD^+	3.0	0.050	0.00044
k_{cat} NADPH/k_{cat} NADH	23.3	0.50	
K_m $NADP^+/K_m$ NAD^+	0.0178	3.4	248
K_m NADPH/K_m NADH	0.086	3.13	
(k_{cat}/K_m $NADP^+$)/(k_{cat}/K_m NAD^+)	168	0.0147	0.0000018
(k_{cat}/K_m NADPH)/(k_{cat}/K_m NADH)	271	0.16	

[a] *Listeria monocytogenes* HMG-CoA reductase data were obtained and analyzed as described in Experimental Procedures and are the average of triplicate determinations. Data for *Archaeoglobus fulgidus* HMG-CoA reductase were derived from ref *11*, and data for *P. mevalonii* HMG-CoA reductase are derived from ref *32*. The k_{cat} value is the number of substrate molecules produced per minute per active site, assumed to be the equivalent of one per monomer. For *L. monocytogenes* HMGR the K_m value is a K' value due to consideration of cooperativity with respect to substrates when calculating kinetic parameters. K_m and K' values are in units of millimolar and k_{cat} is s^{-1}.

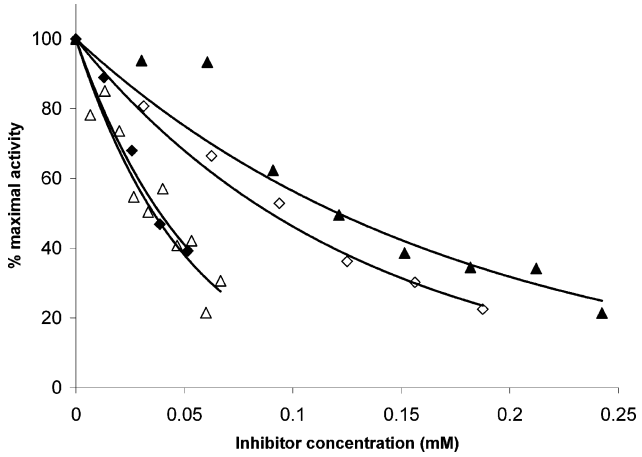

FIGURE 4: Effect of statins on *L. monocytogenes* HMG-CoA reductase activity. Assays were conducted in the presence of increasing concentrations of mevinolin or mevastatin as described in Experimental Procedures. Open triangles: mevinolin. Solid triangles: free acid mevinolin. Open diamonds: mevastatin. Solid diamonds: free acid mevastatin. Experiments were repeated with similar results using different enzyme preparations.

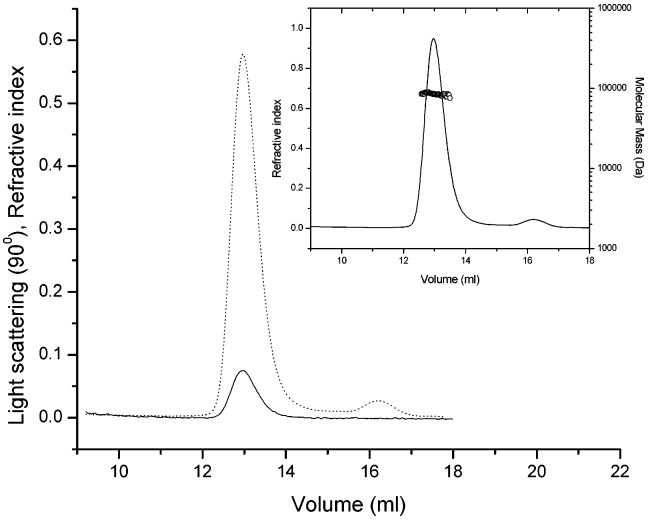

FIGURE 5: Multimeric structure of *L. monocytogenes* HMG-CoA reductase. Listeria HMGR eluted from a Superdex 200 size exclusion column at a volume of 13 mL. Multi-angle laser light scattering and refractive index measurements indicated a molecular mass of 84 900 Da (inset).

more efficient using $NADP^+$ or NADPH, while *A. fulgidus* HMGR is 68 times more efficient with NAD^+ and 6 times more efficient with NADH, for mevalonate oxidation and HMG-CoA reduction, respectively. In general, although both enzymes exhibit dual coenzyme specificity, *L. monocytogenes* HMGR prefers to catalyze NADPH-dependent HMG-CoA reduction and *A. fulgidus* HMGR catalyzes mevalonate oxidation and HMG-CoA reduction with a similar efficiency but with a preference for NAD(H). For comparison, Table 2 also lists kinetic parameters for *P. mevalonii* HMGR, a class II HMGR that preferentially utilizes NAD(H) for catalysis.

Effect of Statins on L. monocytogenes HMG-CoA Reductase. Enzyme assays were conducted on purified *L. monocytogenes* HMGR in the presence of an increasing concentration of each of two statins. Each of the statin compounds, mevinolin or mevastatin, resulted in inhibition of enzyme activity; however, micromolar concentrations were required for significant inhibition. The concentration necessary for 50% inhibition was approximately 30 and 100 μM for the lactone forms and 130 and 30 μM for the acid forms of mevinolin and mevastatin, respectively (Figure 4). Therefore, it was concluded that statin compounds were not effective inhibitors of *L. monocytogenes* HMGR since inhibitory concentrations were more than 1000-fold greater than K_i values for class I forms of the enzyme from rat (*33*), hamster (*16*), and *Haloferax volcanii* (*5*), with K_i values equal to 6, 5, and 15 nM, respectively. Mevinolin, with an estimated K_i of 130 μM for Listeria HMGR, is similarly a poor inhibitor of class II enzymes from *P. mevalonii* and *S. aureus*, with K_i values of 530 mM (*16*) and 320 mM (*10*), respectively, supporting the conclusion that *L. monocytogenes* HMGR is also a class II enzyme.

L. monocytogenes HMG-CoA Reductase is a Multimer in Solution. To assess the multimeric state of *L. monocytogenes* HMGR the enzyme was subjected to Superdex 200 size exclusion chromatography coupled to a multiangle laser light scattering detector. Listeria HMGR eluted at 13 mL from a Superdex 200 gel filtration column and was subjected to multi-angle light scattering and refractive index measurements, which gave an absolute molecular mass of 84900 ± 1700 Da (Figure 5). On the basis of amino acid sequence of the 6×-His-tagged monomer, the calculated molecular mass of the protein is 48.3 kDa, indicating that in solution *L. monocytogenes* HMGR exists as a dimer. The presence of a small peak at an elution of 16 mL suggests that there is some evidence of dissociation of the dimer into single monomer units under these conditions. The multimeric nature of *L. monocytogenes* HMGR is not surprising since all characterized forms of HMGR have been reported to be multimeric. The minimal functional unit of HMGR is believed to be a dimer, as crystal structures (*13*, *34*) and mutagenesis experiments with hamster HMGR (*35*) have shown that amino acids from two separate monomers are necessary to constitute a complete active site. The catalytic domain of human HMGR forms a tetrameric structure (*34*) and *P. mevalonii* HMGR, which crystallizes as a trimer of dimers, has been shown by gel permeation chromatography to be hexameric (*36*).

Does L. monocytogenes Possess an IPP Biosynthesis Operon? The expanding database of genomic sequences has provided a wealth of sequence information about potential routes of IPP synthesis. Upon searching the databases, it is rare to find a eubacterial species in which genes encoding all five enzymes of the mevalonate pathway have been identified. Often a class II HMG-CoA reductase and HMG-CoA synthase have been assigned by the genome projects, but identification of mevalonate kinase, phosphomevalonate kinase, and mevalonate pyrophosphate decarboxylase is less common. Inability to identify these enzymes is due, presumably, to the lack of amino acid sequence conservation and not due to the enzyme not being encoded in the genome. However, in *Borrelia burgdorferi*, the causative agent of Lyme disease, an apparent IPP operon has been identified which encodes each of the five enzymes (Rodwell, V., personal communication). In *L. monocytogenes*, if HMGR functions biosynthetically it is reasonable to assume there would also be genes encoding HMG-CoA synthase, mevalonate kinase, phosphomevalonate kinase, and mevalonate pyrophosphate decarboxylase in addition to HMG-CoA

reductase. However, if these genes are present in the genome are they arranged in an operon? Searching the *Listeria monocytogenes* EGD-e genomic database or conducting a BLAST search using the corresponding enzyme from another eubacterium results in identification of genes that encode proteins assigned as HMG-CoA synthase (accession NP_464940), mevalonate kinase (accession NP_463543), mevalonate pyrophosphate decarboxylase (accession NP_463544), and a second protein with similarity to mevalonate kinase, which may be phosphomevalonate kinase (accession NP_463545). HMG-CoA reductase (genome region 851225−852505) and HMG-CoA synthase (genome region 1445192−1446358) are far away from one another in the genome and in regions with proteins of unknown or unrelated function. The putative mevalonate kinase, phosphomevalonate kinase, and mevalonate pyrophosphate decarboxylase, however, are clustered in the genome region 12918−15874, possibly part of an operon. Analysis of the database genome sequences, therefore, suggests that *L. monocytogenes* likely possesses each of the five enzymes of the mevalonate pathway for the synthesis of IPP.

Analysis of L. monocytogenes HMG-CoA Reductase Three-Dimensional Structure Model. To gain a greater understanding of structure−function relationships in *L. monocytogenes* HMGR, we built a homology model using a sequence alignment with *P. mevalonii* HMGR and the ternary complex structure previously determined for this enzyme (*14*). The 3D structural model contained two monomer subunits that form a dimer, with two flap domains, thought to close over the active site during catalysis (Figure 6A). Energy minimization of the final dimeric structure eliminated unfavorable atomic interactions and electrostatic repulsions. In the modeling procedure, several assumptions were made, including that the minimal functional unit is a dimer, analogous to the *P. mevalonii* enzyme, and that the flap domain (last 50 residues in the sequence) has a similar fold to *P. mevalonii* HMGR and closes over the active site to align the catalytic histidine (His378 in *L. monocytogenes* HMGR) for catalysis. Following modeling of the dimer, docking of the substrate and cofactor was performed to produce a ternary complex approximating a catalytically competent enzyme conformation. Refinement of the ternary complex produced the final model structure with bound HMG-CoA and NAD^+ in the active site (Figure 6A).

From the analysis of the model, it appears that each of the putative conserved catalytic residues are in analogous positions as in *P. mevalonii* HMGR (Figure 6B, 6C). Therefore, it would be reasonable to assume that the amino acids Glu80, Lys264, Asp 280, and His378 of *L. monocytogenes* HMGR play similar roles to their sequence-aligned counterparts in *P. mevalonii* HMGR (Figure 3). However, some amino acid residues interacting with substrates have unique positions in the modeled Listeria HMGR. Notably, instead of a histidine in the second turn of the flap helix there is Gln382 which forms interactions with the NAD(H) pyrophosphate (Figure 6C). In the HMG-CoA binding site Glu80, Lys 264, Asn268 in the active site floor, Asn362 and Arg258 at the top of the active site, and Arg376 which interacts with the pyrophosphate group of HMG-CoA are in similar positions when compared to *P. mevalonii* HMGR, but instead of Arg11, Lys9 of *L. monocytogenes* HMGR forms stacking interactions with the adenine ring and interactions with the 2′-oxygen in the sugar ring (Figure 6D). Additionally Tyr8 forms stacking interactions with the adenine ring of HMG-CoA. Overall, the modeling suggests that *L. monocytogenes* HMGR likely has a 3D structure similar to *P. mevalonii* HMGR.

In the 3D structure of *P. mevalonii* HMGR, which has a 6×10^5-fold greater catalytic efficiency with NAD^+ than with $NADP^+$ (*32*), there is an aspartate (D146) that interacts with the 2′-OH of the adenine ribose, presumably preventing NADP(H) utilization. In *L. monocytogenes*, HMGR a histidine (H143) is aligned with D146 of the Pseudomonas enzyme (Figure 3). In the modeled structure of the Listeria enzyme His143 is present in the region occupied by Asp146 in *P. mevalonii* HMGR. Also, Met186 occupies 3D space near the 2′-OH of the adenine ribose of NAD^+. To facilitate interaction with either NAD(H) or NADP(H), it is possible that changes in the position of His143 and Met186 would accommodate either the 2′-hydroxyl or 2′-phosphate of the adenine ribose, respectively. Notably, histidine would have the ability to form favorable interactions with the 2′-phosphate of NADP(H). It is interesting to note that the 3D structure of the human catalytic domain of HMGR, an NADP(H)-specific enzyme, also has a methionine in the NADP(H)-selective region of the active site (*34*). In addition, methionine is conserved at this position in each of the NADP(H)-utilizing class I forms of HMGR aligned in Figure 3, but the NAD(H)-utilizing *P. mevalonii* HMGR has a threonine aligned with Met186. In a more extensive sequence alignment of approximately 50 HMGR isoforms methonine is present at this position in all but three enzymes, the aforementioned *P. mevalonii* HMGR, the enzyme from *Archaeoglobus fulgidus*, a dual-specificity HMGR that exhibits a preference for NAD(H), and HMGR from *Borrelia burgdorferi*, which remains to be characterized. As reported in Table 2, *L. monocytogenes* HMGR catalytic efficiency is increased approximately 200-fold when NADPH is utilized instead of NADH. The structural model supports the conclusion that this preference for NADPH can be attributed to the presence of His143 in place of Asp146 of *P. mevalonii* HMGR. The potential role of His143 of *L. monocytogenes* HMGR in nicotinamide coenzyme specificity is difficult to discern from sequence alignment, however, since there appears to be no comparable histidine in other class I or class II enzymes (Figure 3). In addition, in a sequence alignment of approximately 50 HMGR isoforms His143 is aligned with a seemingly random assortment of amino acids, possibly due to the low level of amino acid conservation in the region surrounding His143. Whether other class I or class II HMGR isoforms possess an analogous active site histidine will be revealed as more 3D structures become available.

Summary. In this report, we have described the cloning, expression, purification, and kinetic characterization of HMG-CoA reductase from *Listeria monocytogenes*. The enzyme appears to be a class II HMGR based on sequence alignment, sensitivity to statins, and molecular modeling. Kinetic characterization revealed the enzyme exhibits dual coenzyme specificity and can utilize either NAD(H) or NADP(H) in catalysis, but most efficiently catalyzes NADPH-dependent HMG-CoA reduction. Structural modeling suggests the NAD(P)(H) binding site contains a histidine,

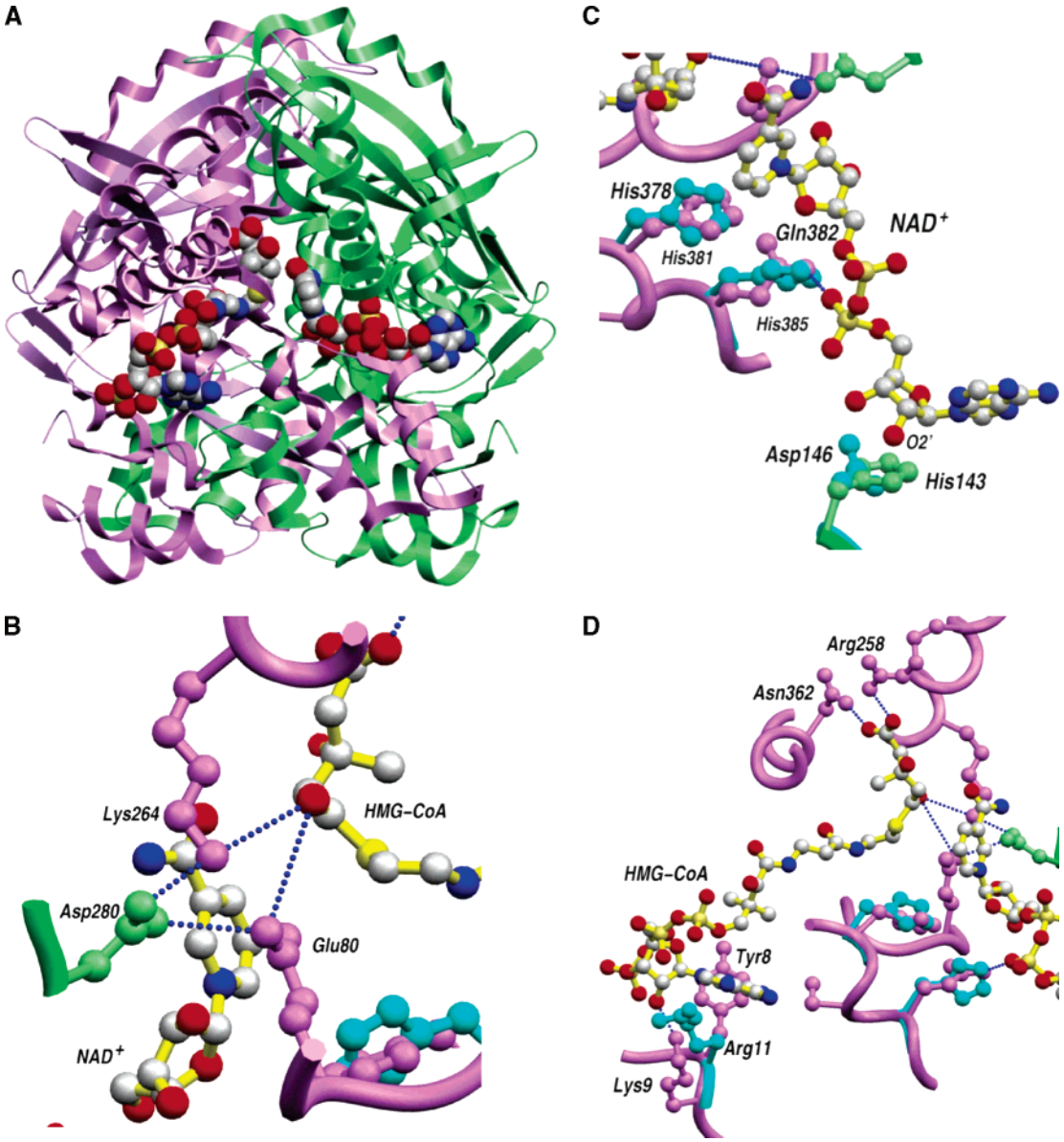

FIGURE 6: (A) 3D structural model of *L. monocytogenes* HMG-CoA reductase. The polypeptide chain is shown in ribbons and the substrates in spacefill, revealing the active site formed by the two monomeric subunits (colored lilac and green). The model was generated by threading onto the existing structure of *P. mevalonii* HMGR (*14*) as described in Experimental Procedures. (B) Atomic interactions in the active site of *L. monocytogenes* HMGR. Active site residues Lys264, Glu80, and Asp280 are represented by balls-and-sticks and colored according to the monomeric subunits. Shown are NAD^+ and HMG-CoA modeled in the active site of *L. monocytogenes* HMGR. Blue dashed lines illustrate interactions between active site residues and the substrates. (C) Selected interactions at the NAD(H) binding site showing *P. mevalonii* HMGR residues in cyan and the analogous residues in *L. monocytogenes* HMGR in lilac and green. His385 from *P. mevalonii* HMGR is replaced in *L. monocytogenes* HMGR by Gln382, which forms a hydrogen bond to an oxygen in the pyrophosphate moiety of NAD(H). Asp146 in the Pseudomonas enzyme is replaced by His143 in the Listeria enzyme, which could potentially allow binding to NADP(H) with an extra phosphate group at the O2′ position. (D) Selected interactions in the HMG-CoA binding site, showing the replacement of Arg11 in *P. mevalonii* HMGR (colored cyan) by Lys9 that interacts with the 2′-oxygen in the sugar ring. Also shown is Tyr8 in *L. monocytogenes* HMGR, which forms stacking interactions with the HMG-CoA adenine ring.

His143, that may interact with the 2′ phosphate of the adenine ribose of NADP(H), in contrast to the NAD(H)-dependent HMGR from *P. mevalonii* which has an aspartate at this position. A potential future investigation would employ site-directed mutagenesis to change His143 to aspartate, which would be predicted to significantly decrease the ability of *L. monocytogenes* HMGR to utilize NADPH in catalysis. This and other future studies on catalysis by the enzyme and solution of the 3D structure may provide information useful for designing inhibitors of *L. monocytogenes* HMGR, helping to prevent growth of this pathogenic organism.

ACKNOWLEDGMENT

The authors thank Tom Jowitt for assistance with light scattering experiments and Dr. Brian Wilkinson for providing a culture of *Listeria monocytogenes* EGD-e.

SUPPORTING INFORMATION AVAILABLE

Initial velocity versus substrate concentration plots used to derive the kinetic parameters reported in this study. This material is available free of charge via the Internet at http://pubs.acs.org.

REFERENCES

1. Bochar, D. A., Stauffacher, C. V., and Rodwell, V. W. (1999) Sequence comparisons reveal two classes of 3-hydroxy-3-methylglutaryl coenzyme A reductase, *Mol. Genet. Metab. 66*, 122−127.
2. Mayer, R. J., Debouck, C., and Metcalf, B. W. (1988) Purification and properties of the catalytic domain of human 3-hydroxy-3-methylglutaryl-CoA reductase expressed in *Escherichia coli*, *Arch. Biochem. Biophys. 267*, 110−118.
3. Frimpong, K., Darnay, B. G., Rodwell, V. W. (1993) Syrian hamster 3-hydroxy-3-methylglutaryl-coenzyme A reductase expressed in *Escherichia coli*: production of homogeneous protein, *Prot. Expr. Purif. 4*, 337−344.
4. Basson, M. E., Thorsness, M., and Rine, J. (1986) Saccharomyces cerevisiae contains two functional genes encoding 3-hydroxy-3-methylglutaryl-coenzyme A reductase, *Proc. Natl. Acad. Sci. U.S.A. 83*, 5563−5567.
5. Bischoff, K. M., and Rodwell, V. W. (1996) 3-Hydroxy-3-methylglutaryl-coenzyme A reductase from *Haloferax volcanii*: purification, characterization, and expression in *Escherichia coli*, *J. Bacteriol. 178*, 19−23.
6. Bochar, D. A., Brown, J. R., Doolittle, W. F., Klenk, H. P., Lam, W., Schenk, M. E., Stauffacher, C. V., and Rodwell, V. W. (1997) 3-Hydroxy-3-methylglutaryl coenzyme A reductase of *Sulfolobus solfataricus*: DNA sequence, phylogeny, expression in *Escherichia coli* of the hmgA gene, and purification and kinetic characterization of the gene product, *J. Bacteriol. 179*, 3632−3638.
7. Hedl, M., Tabernero, L., Stauffacher, C., and Rodwell, V. (2004) Class II 3-Hydroxy-3-methylglutaryl coenzyme A reductases, *J. Bacteriol. 186*, 1927−1932.
8. Beach, M. J., and Rodwell, V. W. (1989) Cloning, sequencing, and overexpression of mvaA, which encodes *Pseudomonas mevalonii* 3-hydroxy-3-methylglutaryl coenzyme A reductase, *J. Bacteriol. 171*, 2994−3001.
9. Takahashi, S., Kuzuyama, T., and Seto, H. (1999) Purification, characterization, and cloning of a eubacterial 3-hydroxy-3-methylglutaryl coenzyme A reductase, a key enzyme involved in biosynthesis of terpenoids, *J. Bacteriol. 181*, 1256−1263.
10. Wilding, E. I., Kim, D. Y., Bryant, A. P., Gwynn, M. N., Lunsford, R. D., McDevitt, D., Myers, J. E., Jr., Rosenberg, M., Sylvester, D., Stauffacher, C. V., and Rodwell, V. W. (2000) Essentiality, expression, and characterization of the class II 3-hydroxy-3-methylglutaryl coenzyme A reductase of *Staphylococcus aureus*, *J. Bacteriol. 182*, 5147−5152.
11. Kim, D. Y., Stauffacher, C. V., and Rodwell, V. W. (2000) Dual coenzyme specificity of *Archaeoglobus fulgidus* HMG-CoA reductase, *Protein Sci. 9*, 1226−1234.
12. Gill, J. F., Jr., Beach, M. J., and Rodwell, V. W. (1985) Mevalonate utilization in *Pseudomonas sp. M.* Purification and characterization of an inducible 3-hydroxy-3-methylglutaryl coenzyme A reductase, *J. Biol. Chem. 260*, 9393−9398.
13. Lawrence, C. M., Rodwell, V. W., and Stauffacher, C. V. (1995) Crystal structure of *Pseudomonas mevalonii* HMG-CoA reductase at 3.0 angstrom resolution, *Science 268*, 1758−1762.
14. Tabernero, L., Bochar, D. A., Rodwell, V. W., Stauffacher, C. V. (1999) Substrate-induced closure of the flap domain in the ternary complex structures provides insights into the mechanism of catalysis by 3-hydroxy-3-methylglutaryl-CoA reductase, *Proc. Natl. Acad. Sci. U.S.A. 96*, 7167−7171.
15. Friesen, J. A., and Rodwell, V. W. (2004) The 3-hydroxy-3-methylglutaryl coenzyme A (HMG-CoA) reductases, *Genome Biol. 5*, 248.
16. Rodwell, V. W., Beach, M. J., Bischoff, K. M., Bochar, D. A., Darnay, B. G., Friesen, J. A., Gill, J. F., Hedl, M., Jordan-Starck, T., Kennelly, P. J., Kim, D. Y., and Wang, Y. (2000) 3-Hydroxy-3-methylglutaryl-CoA reductase, *Methods Enzymol. 324*, 259−280.
17. Rohmer, M., Knani, M., Simonin, P., Sutter, B., and Sahm, H. (1993) Isoprenoid biosynthesis in bacteria: a novel pathway for the early steps leading to isopentenyl diphosphate, *Biochem. J. 295*, 517−524.
18. Boucher, Y., and Doolittle, W. F. (2000) The role of lateral gene transfer in the evolution of isoprenoid biosynthesis pathways, *Mol. Microbiol. 37*, 703−716.
19. Rodriguez-Concepcion, M., and Boronat, A. (2002) Elucidation of the methylerythritol phosphate pathway for isoprenoid biosynthesis in bacteria and plastids. A metabolic milestone achieved through genomics, *Plant Physiol. 130*, 1079−1089.
20. Begley, M., Gahan, C. G., and Hill, C. (2002) Bile stress response in *Listeria monocytogenes* LO28: adaptation, cross-protection, and identification of genetic loci involved in bile resistance, *Appl. Environ. Microbiol. 68*, 6005−6012.
21. Glaser, P., Frangeul, L., Buchrieser, C., Rusniok, C., Amend, A., Baquero, F., Berche, P., Bloecker, H., Brandt, P., Chakraborty, T., Charbit, A., Chetouani, F., Couve, E., de Daruvar, A., Dehoux, P., Domann, E., Dominguez-Bernal, G., Duchaud, E., Durant, L., Dussurget, O., Entian, K. D., Fsihi, H., Garcia-del Portillo, F., Garrido, P., Gautier, L., Goebel, W., Gomez-Lopez, N., Hain, T., Hauf, J., Jackson, D., Jones, L. M., Kaerst, U., Kreft, J., Kuhn, M., Kunst, F., Kurapkat, G., Madueno, E., Maitournam, A., Vicente, J. M., Ng, E., Nedjari, H., Nordsiek, G., Novella, S., de Pablos, B., Perez-Diaz, J. C., Purcell, R., Remmel, B., Rose, M., Schlueter, T., Simoes, N., Tierrez, A., Vazquez-Boland, J. A., Voss, H., Wehland, J., and Cossart, P. (2001) Comparative genomics of Listeria species, *Science 294*, 849−852.
22. Tabernero, L., Rodwell, V. W., and Stauffacher, C. V. (2003) Crystal structure of a statin bound to a class II hydroxymethylglutaryl-CoA reductase, *J. Biol. Chem. 30*, 19933−19938.
23. Bradford, M. M. (1976) A rapid and sensitive method for the quantitation of microgram quantities of protein utilizing the principle of protein-dye binding, *Anal. Biochem. 72*, 248−254.
24. Segel, L. H. (1975) *Enzyme Kinetics. Behavior and Analysis of Rapid Equilibrium and Steady-State Enzyme Systems*, John Wiley & Sons, New York.
25. Bergdahl, A., Persson, E., Hellstrand, P., and Sward, K. (2003) Lovastatin induces relaxation and inhibits L-type Ca^{2+} current in the rat basilar artery, *Pharmacol. Toxicol. 93*, 128−134.
26. Levitt, M. (1992) Accurate modeling of protein conformation by automatic segment matching, *J. Mol. Biol. 226*, 507−533.
27. Brunger, A. T., Adams, P. D., Clore, G. M., DeLano, W. L., Gros, P., Grosse-Kunstleve, R. W., Jiang, J. S., Kuszewski, J., Nilges, N., Pannu, N. S., Read, R. J., Rice, L. M., Simonson, T., and Warren, G. L. (1998) Crystallography and NMR system (CNS): A new software system for macromolecular structure determination, *Acta Crystallogr. D54*, 905−921.
28. Wang, Y., Darnay, B. G., and Rodwell, V. W. (1990) Identification of the principal catalytically important acidic residue of 3-hydroxy-3-methylglutaryl coenzyme A reductase, *J. Biol. Chem. 265*, 21634−21641.
29. Bochar, D. A., Tabernero, L., Stauffacher, C. V., and Rodwell, V. W. (1999) Aminoethylcysteine can replace the function of the essential active site lysine of *Pseudomonas mevalonii* 3-hydroxy-3-methylglutaryl coenzyme A reductase, *Biochemistry 38*, 8879−8883.
30. Darnay, B. G., Wang, Y., and Rodwell, V. W. (1992) Identification of the catalytically important histidine of 3-hydroxy-3-methylglutaryl-coenzyme A reductase, *J. Biol. Chem. 267*, 15064−15070.
31. Sato, R., Goldstein, J. L., and Brown, M. S. (1993) Replacement of serine-871 of hamster 3-hydroxy-3-methylglutaryl-CoA reductase prevents phosphorylation by AMP-activated kinase and blocks inhibition of sterol synthesis induced by ATP depletion, *Proc. Natl. Acad. Sci. U.S.A. 90*, 9261−9265.
32. Friesen, J. A., Lawrence, C. M., Stauffacher, C. V., and Rodwell, V. W. (1996) Structural determinants of nucleotide coenzyme specificity in the distinctive dinucleotide binding fold of HMG-CoA reductase from *Pseudomonas mevalonii*, *Biochemistry 35*, 11945−11950.
33. Alberts, A. W., Chen, J., Kuron, G., Hunt, V., Huff, J., Hoffman, C., Rothrock, J., Lopez, M., Joshua, H., Harris, E., Patchett, A.,

Monaghan, R., Currie, S., Stapley, E., Albers-Schonberg, G., Hensens, O., Hirshfield, J., Hoogsteen, K., Liesch, J. S., and Springer, J. (1980) Mevinolin: A highly potent competitiveinhibitor of hydroxymethylglutaryl-coenzyme A reductase and a cholesterol-lowering agent, *Proc. Natl. Acad. Sci. U.S.A. 77*, 3957−3961.

34. Istvan, E. S., Palnitkar, M., Buchanan, S. K., and Deisenhofer, J. (2000) Crystal structure of the catalytic portion of human HMG-CoA reductase: insights into regulation of activity and catalysis, *EMBO J. 19*, 819−8309.

35. Frimpong, K., and Rodwell, V. W. (1994) The active site of hamster 3-hydroxy-3-methylglutaryl-CoA reductase resides at the subunit interface and incorporates catalytically essential acidic residues from separate polypeptides, *J. Biol. Chem. 269*, 1217−1221.

36. Rogers, K. S., Rodwell, V. W., and Geiger, P. (1997) Active form of *Pseudomonas mevalonii* 3-hydroxy-3-methylglutaryl coenzyme A reductase, *Biochem. Mol. Med. 61*, 114−120.

BI0614636